A Compressed Sensing Approach for Biological Microscopy Image Denoising

Marcio M. Marim, Elsa D. Angelini, Jean-Christophe Olivo-Marin

A Compressed Sensing Approach for Biological Microscopy Image Denoising

Marcio M. Marim[*1] Elsa D. Angelini[§2], J.-C. Olivo-Marin[*3]
[*]Institut Pasteur, Unité d'Analyse d'Images Quantitative CNRS URA 2582, F-75015 Paris
[§]Institut TELECOM, TELECOM ParisTech CNRS LTCI, F-75013 Paris

Abstract—**Compressed Sensing (CS) provides a new framework for signal sampling, exploiting redundancy and sparsity in incoherent bases. For images with homogeneous objects and background, CS provides an optimal reconstruction framework from a set of random projections in the Fourier domain, while constraining bounded variations in the spatial domain. In this paper, we propose a CS-based method to simultaneously acquire and denoise data based on statistical properties of the CS optimality, signal modeling and characteristics of noise reconstruction. Our approach has several advantages over traditional denoising methods, since it can under-sample, recover and denoise images simultaneously. We demonstrate with simulated and practical experiments on fluorescence images that we obtain images with similar or increased SNR even with reduced exposure times. Such results open the gate to new mathematical imaging protocols, offering the opportunity to reduce exposure time along with photo-toxicity and photo-bleaching and assist biological applications relying on fluorescence microscopy.**

I. INTRODUCTION

In microscopy, observation of fluorescent molecules is challenged by the photo-bleaching and photo-toxicity, as these molecules are slowly destroyed by the light exposure necessary to stimulate them into fluorescence. Unfortunately, reducing exposure time drastically deteriorates the signal to noise ratio (SNR) and hence, the image quality. To improve the SNR, many denoising methods are available such as *Non-Local Means* (NL-means) [1], *Total Variation* (TV) [2], non-linear isotropic and anisotropic diffusion [3]. Other methods exploit the decomposition of the data into the wavelets, ridglets, curvelets bases and perform denoising by shrinking the transform coefficients [4]. Recently, efficient denoising methods were also developed based on sparsity and redundant representations over learned dictionaries, where the image is denoised and a dictionary is trained simultaneously (e.g. the K-SVD [5]).

In this paper we propose an application of Compressed Sensing on fluorescence microscopy images, enabling the acquisition of high SNR images under reduced exposure times. Instead of post-acquisition denoising methods, here we are interested in denoising as much as CS advantages. Our framework is based on the property of CS to efficiently reconstruct sparse signals with under-sampled acquisition rates, significantly below the Shannon/Nyquist theoretical bound. Similarly to recent experiments for MRI CS-based reconstruction [6], the acquisition protocol consists in measuring the image signal onto a random set of Fourier vectors [7] and constraining *Total Variation* (TV), which is incoherent to the Fourier domain. Indeed, the CS framework introduced by Candès [8] provides theoretical results and shows that if a signal is sparse (i.e. has a small number of non-zero coefficients) in some basis, then with high probability, uniform random projections of this signal onto an unstructured domain, where the signal is not sparse, contains enough information to optimally reconstruct this signal. The incoherence property between the sparsity

basis Ψ and the sampling basis Φ ensures that signals having sparse representations in Ψ must have a large support in the measurement domain described by Φ. Random selections of basis functions in Φ are typically suitable since random vectors are, with very high probability, incoherent with any sparsity-encoding basis functions from Ψ, defining orthogonal domains [9].

Considering that a noisy signal x has a sparse representation in some basis Ψ, we want to recover the signal $x \in \mathbb{R}^N$ from noisy measurements $y = \Phi(x + n) \mid y \in \mathbb{R}^M$, the sampling matrix being defined by M vectors in Φ, with $M \ll N$. The presence of noise in the acquired signal might alter its sparsity in the domain Ψ. By optimally reconstructing a signal with explicit sparsity constraints, CS offers a theoretical framework to remove non-sparse random noise components from a corrupted signal. Indeed, removing noise from $x + n$ will rely on the efficacy of Ψ on representing the signal x sparsely and the inefficacy on representing the noise n [10]. We propose to use the CS sampling and reconstruction framework to denoise and improve the SNR of microscopy fluorescence images acquired using shorter exposure times.

II. BACKGROUND

A. Sparsity and incoherence

A discrete signal is considered sparse when it has a large number of zero coefficients on some basis functions. We define a S-sparse signal if S elements are non-zero. Natural signals measuring discrete events or natural images with smooth and homogeneous objects can be considered approximately sparse in some basis and be accurately approximated with a small set of coefficients [7], [11]. In the general case, a signal has a S-sparse representation in the set of basis functions $\Psi = \{\Psi_i\}_{i=1}^N$ if:

$$x = \sum_i c_i \Psi_i \qquad \text{with} \parallel c \parallel_{\ell_1} \approx S \tag{1}$$

Here Ψ_i is a basis function and the ℓ_1 norm well approximates the number of nonzero coefficients of c.

In our framework, for biological images, we choose the global *Total Variation* as sparsifying transform [12], [13]. This measure is well-known in image processing and very popular in variational segmentation problems for its ability to limit high frequencies and to provide regularized segmented regions. This measure is also well suited for denoising where the goal is to restore an image with smooth objects and background. Minimization of the TV norm, introduced in [14], [2] for signal denoising, corresponds to a constraint on the number of discontinuities in an image, and the homogeneity of the objects. TV sparsity constraints in CS were introduced by Candès in [8], expressed as:

$$TV(x) = \parallel \nabla(x) \parallel_{\ell_1} \tag{2}$$

$$TV(x) = \sum_{i,j} \sqrt{\{x_{(i+1,j)} - x_{(i,j)}\}^2 + \{x_{(i,j+1)} - x_{(i,j)}\}^2} \tag{3}$$

[1]M. Marim: marim@pasteur.fr
[2]E. D. Angelini: elsa.angelini@telecom-paristech.fr
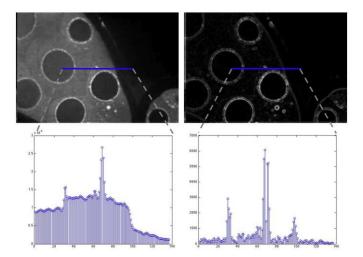[3]J.-C. Olivo-Marin: jcolivo@pasteur.fr, www.bioimageanalysis.org

Fig. 1. Image sparsity illustrated in a two-dimensional spatial domain. Top left: original image. Top right: nearly sparse representation domain (using the gradient of the signal). Bottom: line profiles from corresponding blue lines in the spatial and gradient domains.

It is interesting to note here, as pointed out in [8], that the transform which produces the TV coefficients corresponds to the ℓ_2 norm of a particular operation on the image, based on the computation of horizontal ∇_x and vertical ∇_y gradients and combination of these operators into a complex-valued image: $\nabla_x + i\nabla_y$. The TV coefficients are then the ℓ_2 norm of this transformed image (computed locally for each pixel) and the CS framework minimizes the global ℓ_1 norm of these TV coefficients over the whole image. Such transform corresponds to the decomposition of the image onto *Heavisides* basis functions, which support is adaptive (similarly to the *Basis Pursuit* framework for decompositions on dictionaries [11]) and defined by the localization of high-gradient values in the image (i.e. edge maps). TV constraint is well suited for biological images, where structures and background provide small gradient values while a finite set of edges provides high gradient values as illustrated in Figure 1 for drosophila ovocytes.

The design of the sampling matrix Φ must enforce incoherence between the acquisition and the sparsity domain. This constraint has been formulated though several criteria, based on mutual coherence measures [12], [10], or matrix properties such as the Restricted Isometry Property (RIP) conditions described in [7]. Random acquisition in the Fourier domain, encoded by a matrix with 1s and 0s at random frequency locations verifies this incoherence property when combined with TV spatial constraints.

III. METHOD

A. Reconstruction from noisy measurements

In the context of noisy measurements $y = \Phi(x + n)$, which is the case for microscopy images corrupted with acquisition noise, we wish to recover only the signal component $x \in \mathbb{R}^N$. If we make the assumptions that the noise energy is bounded by a known constant $\| n \|_{\ell_2} \leq \epsilon$, the transformed signal Ψx is sparse, and $\Phi \in \mathbb{R}^{MN}$ is a random matrix sampling x in the Fourier domain, the true signal component x can be recovered nearly exactly using the following convex optimization:

$$\hat{x} = \arg \min_{x \in \mathbb{R}^N} \| \Psi x \|_{\ell_1} \text{ s.t. } \| y - \Phi x \|_{\ell_2} \leq \delta \qquad (4)$$

for some small $\delta \geq \epsilon$. In [15] it was shown that the solution $\hat{x}$ is guaranteed to be within $C\delta$ of the original signal x.

$$\| \hat{x} - x \|_{\ell_2} \leq C\delta \qquad \text{with } C > 0 \qquad (5)$$

We note here that this CS-based estimation framework, with noisy observations and TV spatial constraints, guarantees that no false component of $x + n$ with significant energy is created as it minimizes its ℓ_1 norm, which is particularly high for additive random noise components. More specifically, the TV-based spatial sparsity constraint, will lead to smooth edges and removal of noise components, resulting in an error:

$$\| \hat{x} - x \|_{\ell_2} \leq \alpha + \beta \qquad (6)$$

where α reflects the desired error (responsible for noise removal) from the relaxation of the constrain δ in (4) and β reflects the undesired error from smooth edges of signal. If TV represents x efficiently and n inefficiently, the term β vanishes and $\alpha \to C\delta$.

B. The recovery algorithm

As an alternative to acquisition problems we focus on utilizing dual sparse and redundant representations in the CS framework for fluorescence microscopy image denoising via two separate schemes.

A first strategy consists in acquiring K images $x_i + n_i$ (with Φ_i matrices) exposed T/K ms, restoring each one independently (equation 7) and combining the K restoration results into a single denoised image. This scheme exploits the fact that fluorescence signal $\Phi_i x_i$ should be strongly correlated in all acquisitions, while noisy components $\Phi_i n_i$ should not be.

$$\hat{x}_i = \arg \min_{x \in \mathbb{R}^N} \| \Psi x_i \|_{\ell_1} \text{ s.t. } \| y_i - \Phi_i x_i \|_{\ell_2} \leq \delta \qquad (7)$$

where $y_i = \Phi_i(x_i + n_i)$ for $i = 1...K$.

A second CS denoising scheme is proposed, which consists in determining the exposure time X necessary to obtain, with a set of combined CS restorations, a target SNR level, corresponding to the SNR measured on the image exposed T ms. This scheme provides the potential advantage of requiring a single shorter acquisition time, limiting degradation of the biological material through photo-toxicity and photo-bleaching.

Combining CS reconstructions implies a sequence of CS reconstructions of a single noisy image acquisition $x + n$, using different sampling matrices Φ_i, as described below:

$$\hat{x}_i = \arg \min_{x \in \mathbb{R}^N} \| \Psi x \|_{\ell_1} \text{ s.t. } \| y_i - \Phi_i x \|_{\ell_2} \leq \delta \qquad (8)$$

for $i = 1...K$. The last step of both algorithms involves the combination of $\hat{x}_i$ by averaging to generate a final denoised image $\hat{x}$.

C. CS and scalability

The degrees of freedom in this series of CS experiments are in the design of the sampling matrix Φ: the number of random measurements M and their location in the Fourier domain. The CS theoretical framework states that the more measurements are used in the Φ domain, the closer is the reconstructed signal to the original measured signal. In the context of denoising (rather than estimation) we have a dual constraint on the estimation of true signal component and the risk to reconstruct noisy components. Indeed, for a single CS experiment, the fluorescence signal will generate, from a set of random measures of structured Fourier values, a restored image with high values depicting a good estimation of the true signal. At the same time, purely random noisy component will
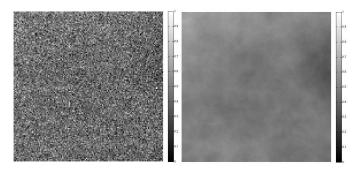
Fig. 3. Left: Pure noise image extracted from a microscopy image background. Right: Result obtained averaging 20 images recovered with different sets of measurements Φ_i for ($i = 1...20$).

be interpreted, from a set of undifferentiated Fourier values, as a structured combination of oscillating components, extrapolated over the spatial domain into patches, under the regularizing TV effect. Noise patches and fluorescence spatial localization will be directly related to M, the number of CS measurements acquired by Φ. We illustrate in Figure 2 how this number of measurements can be naturally viewed as a scale parameter where small scales enable more noise reconstruction.

In the experiment on Figure 2, we observe that noise component is more uncorrelated than signal across scales while the signal component spatial resolution decreases.

We can make a connection here to the family of multi-scale transforms [16]. These transforms were theoretically defined as linear transforms with a scale parameter controlling the ability of the transform to simplify the signal. We know from the sparsity TV constraint that strong signal recovered by the CS framework will correspond to strong underlying true signal components. Therefore, CS does not introduce false signal components and fits well in the framework of multi-scale transforms, as illustrated in Figure 2. Indeed it appears that such multi-scale CS approach verify scale space properties such as simplifications, homogeneity, isotropy as well as rotational and shift invariance.

If results from CS recovery of a purely noise signal are combined, the mean intensity results in a nearly homogeneous signal, as illustrated in Figure 3. This observation clearly justifies the averaging operator introduced in Section III-B to remove noise from images.

IV. EXPERIMENTAL RESULTS

A. Noise removal and recovered images

Results from the first scheme of denoising are ilustrated in Figure 4 are detailed in table I and results from the second scheme of denoising are ilustrated in Figure 5 and are detailed in table II. In all experiments, important improvements of the SNR or the exposure time were achieved.

For experiments on drosophila cells image (Figure 4 and 5), the SNR was highly improved and details were very well preserved. The algorithm shows its efficacy and importance on microscopy applications, where photons detected are limited and image quality is normally degraded. The improvement can be provided in two different ways, fixing the desired SNR and reducing the exposure time, or fixing the exposure time and improving the SNR, as the denoised images in Figure 5 (middle) illustrate.

We have performed a comparison of our method with exclusive *Total Variation* denoising methods. The algorithm used for this comparison is the one presented by Gilboa et al. in [17]. This algorithm minimizes TV in two schemes 1. with global variance

Exposure Time	CNR	SNR
100 ms	30.00	6.42
10 ms	5.17	3.61
$10 \cdot 10$ ms $+ 10 \cdot$ CS	96.60	13.31

TABLE I
RESULTS FROM CS-BASED DENOISING OF THE IMAGE ON FIGURE 4 BY THE METHOD DESCRIBED ON SECTION III-B.

Exposure Time	CNR	SNR
100 ms	30.00	6.42
100 ms $+ 1 \cdot$ CS	36.50	7.24
100 ms $+ 10 \cdot$ CS	90.23	11.02

TABLE II
RESULTS FROM CS-BASED DENOISING OF THE IMAGE ON FIGURE 5 BY THE METHOD DESCRIBED ON SECTION III-B.

constraints (scalar fidelity term) and 2. in order to preserve texture and small scale details, using an adaptive variational scheme that controls the level of denoising by local variance constraints (adaptive fidelity term). Residuals and SNR results in Figure 6 shows that CS is able to discriminate noise from signal more than exclusive TV minimization methods. This is justified by the reason that CS has both TV minimization constraint, and uncorrelated noise recovery. Differences on each set of under-sampled random projections establish strongest constraint for signal-measures fidelity than for noise-measures fidelity.

V. CONCLUSION

We introduce a Compressed Sensing-based image acquisition and denoising method exploiting multiple reconstructions with random Fourier projections. Our approach presents several advantages over traditional denoising methods, joining image acquisition, CS advantages and denoising in one framework. In the context of biological imaging, experiments demonstrated improvements of SNR values up to a factor of 2 on microscopy images acquired with limited exposure times. These results also open the gate to new microscopy acquisition schemes, enabling for instance better control on cells photo-toxicity and photo-bleaching of fluorescent targets.
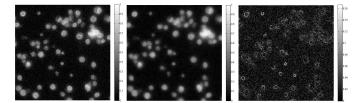
ACKNOWLEDGMENT

Fig. 5. Left: Noisy image x of drosophila cells imaged by fluorescent microscopy, $SNR = 6.42$ and exposure time $t = 100ms$. Middle: Denoised image $\hat{x}$, composed from 10 images recovered with different measurements, as the second scheme proposed on Section III-B, $SNR = 11.02$. Right: Residual $\| \hat{x} - x \|_{l2}$.
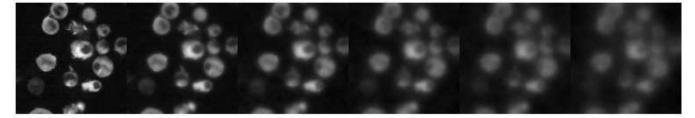
Fig. 2. Average image recovered with six different numbers of measurements (i.e. 6 scales). Scales varies from a compression ratio exponentially increasing from $M = 30\%$ to $M = 0.3\%$.
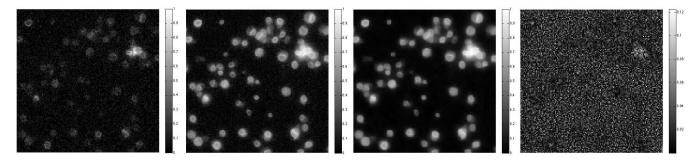

Fig. 4. Left: One noisy image x_i of drosophila cells imaged by fluorescent microscopy, $SNR = 3.61$ and exposure time $t = 10ms$. Middle left: Image acquired with exposure time equal to $t = 100ms$ and $SNR = 6.42$. Middle right: Denoised image $\hat{x}$, composed from 10 images recovered from 10 images with exposure time $t = 10ms$, as the first scheme proposed on Section III-B, $SNR = 13.31$. Right: Residual $\parallel \hat{x} - I_{100ms} \parallel_{l_2}$.
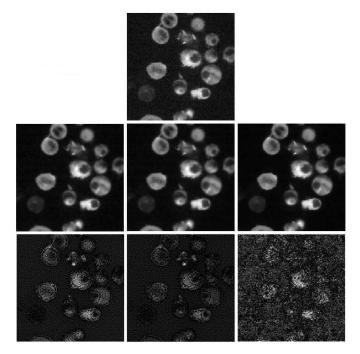

Fig. 6. Top: Noisy original image x of lymphocytes imaged by fluorescent microscopy, $SNR = 8.14$. Middle left: Denoised image by scalar TV, $SNR = 11.2$. Middle: Denoised image by adaptive TV, $SNR = 12.5$. Middle right: Denoised image $\hat{x}$ with CS, composed from 10 images recovered with different sets of measurements, $SNR = 14.28$. Bottom: Images from residuals of all respective methods $\parallel \hat{x} - x \parallel_{\ell_2}$.

REFERENCES

[1] A. Buades, B. Coll, and J. Morel, "A review of image denoising algorithms, with a new one," *Multiscale Modeling and Simulation (SIAM interdisciplinary journal)*, vol. 4 (2), pp. 490–530, 2005.

[2] L. I. Rudin, S. Osher, and E. Fatemi, "Nonlinear total variation based noise removal algorithms*," *Physica D*, vol. 60, pp. 259–268, 1992.

[3] J. Weickert, B. T. H. Romeny, and M. Viergever, "Efficient and reliable schemes for nonlinear diffusion filtering," *IEEE Trans. Image Processing*, vol. 7, pp. 398–410, 1998.

[4] R. DeVore and B. Lucier, "Fast wavelet techniques for near-optimal processing," *IEEE Military Communications Conference, New York*, pp. 48.3.1–48.3.7, 1992.

[5] M. Aharon, M. Elad, and A. Bruckstein, "The K-SVD algorithm," *Proceedings of SPARSE'05, Rennes, France*, november 2005.

[6] M. Lustig, D. Donoho, and J. M. Pauly, "Sparse MRI: The application of compressed sensing for rapid MR imaging," *Magnetic Resonance in Medicine*, vol. 58(6), pp. 1182–1195, December 2007.

[7] E. Candès, J. Romberg, and T. Tao, "Robust uncertainty principles: Exact signal reconstruction from highly incomplete frequency information," *IEEE Trans. on Information Theory*, vol. 52(2), pp. 489–509, June 2006.

[8] E. Candès and J. Romberg, "Practical signal recovery from random projections," in *Proceedings of the SPIE Conference on Wavelet Applications in Signal and Image Processing XI*, San Jose, California, January 2005, p. 5914.

[9] D. L. Donoho, "Compressed sensing," *IEEE Trans. on Information Theory*, vol. 52(4), pp. 1289–1306, April 2006.

[10] D. Donoho, M. Elad, and V. Temlyakov, "Stable recovery of sparse overcomplete representations in the presence of noise," *IEEE Transactions on Information Theory*, vol. 52, pp. 6–18, January 2006.

[11] S. S. Chen, D. L. Donoho, and M. A. Saunders, "Atomic decomposition by basis pursuit," *SIAM Journal on Scientific Computing*, vol. 20, no. 1, pp. 33–61, February 1998.

[12] E. Candès and J. Romberg, "Sparsity and incoherence in Compressive Sampling," *Inverse Problems*, vol. 23(3), pp. 969–985, November 2006.

[13] A. Cohen, R. DeVore, P. Petrushev, and H. Xu, "Nonlinear approximation and the space BV($\mathbb{R}^2$)^1," *American Journal of Mathematics*, vol. 121, pp. 587–628, 1999.

[14] T. F. Chan, S. Osher, and J. Shen, "The digital TV filter and nonlinear denoising," *IEEE Transactions on Image Processing*, vol. 10(2), pp. 231–241, February 2001.

[15] E. Candès, J. Romberg, and T. Tao, "Stable signal recovery from incomplete and inaccurate measurements," *Communications on Pure and Applied Mathematics*, vol. 59(8), pp. 1207–1223, August 2006.

[16] T. Lindeberg, *Scale-Space Theory in Computer Vision*. The Kluwer International Series in Engineering and Computer Science, Dordrecht: Kluwer Academic, 1994.

[17] G. Gilboa, N. Sochen, and Y. Y. Zeevi, "Texture preserving variational denoising using an adaptive fidelity term," *IEEE Trans. on Image Processing*, vol. 15(8), pp. 2281–2289, 2006.